LETTER

Corrected: Publisher Correction

https://doi.org/10.1038/s41586-018-0432-4

Magnetoelectric inversion of domain patterns

N. Leo[1,2,12], V. Carolus[3,12], J. S. White[4], M. Kenzelmann[4], M. Hudl[5], P. Tolédano[6], T. Honda[7], T. Kimura[8], S. A. Ivanov[9], M. Weil[10], Th. Lottermoser[1], D. Meier[11] & M. Fiebig[1]*

The inversion of inhomogeneous physical states has great technological importance; for example, active noise reduction relies on the emission of an inverted sound wave that interferes destructively with the noise of the emitter[1], and inverting the evolution of a spin system by using a magnetic-field pulse enables magnetic resonance tomography[2]. In contrast to these examples, inversion of a distribution of ferromagnetic or ferroelectric domains within a material is surprisingly difficult: field poling creates a single-domain state, and piece-by-piece inversion using a scanning tip is impractical. Here we report inversion of entire ferromagnetic and ferroelectric domain patterns in the magnetoelectric material Co_3TeO_6 and the multiferroic material Mn_2GeO_4, respectively. In these materials, an applied magnetic field reverses the magnetization or polarization, respectively, of each domain, but leaves the domain pattern intact. Landau theory indicates that this type of magnetoelectric inversion is universal across materials that exhibit complex ordering, with one order parameter holding the memory of the domain structure and another setting its overall sign. Domain-pattern inversion is only one example of a previously unnoticed effect in systems such as multiferroics, in which several order parameters are available for combination. Exploring these effects could therefore advance multiferroics towards new levels of functionality.

Since their discovery in the 1950s, multiferroics—materials in which magnetic and ferroelectric order coexist—have undergone tremendous development[3,4]. This is partly due to the desire to control magnetism by using electric rather than magnetic fields. However, any such magnetoelectric correlation must be permitted by the order and symmetry of the material. Particularly complex magnetoelectric coupling may therefore require the presence of several, often multidimensional, order parameters; for example, the coexistence of a large magnetization and polarization in hybrid improper ferroelectrics involves three order parameters[5]. Even more parameters are required if an additional condition that the magnetization and polarization are parallel is introduced[6]. In addition to coupled magnetic and electric order, the interplay of so many order parameters could yield other valuable properties, which have yet to be discovered.

Here, we use the versatility that results from the large number of magnetic and electric order parameters to achieve inversion of an entire ferromagnetic or ferroelectric multi-domain pattern in a single step: a homogeneous field reverses the magnetization or polarization of each domain, but preserves the original domain pattern. To demonstrate the universal nature of such inversion, we select two materials with different properties—magnetoelectric Co_3TeO_6 and multiferroic Mn_2GeO_4. Using these materials, we demonstrate inversion of a ferromagnetic and a ferroelectric domain pattern, respectively, by imaging the domain structure using optical second-harmonic generation (SHG)[7,8]. Analysis of the free energy reveals that in both compounds, one order parameter holds the memory of the domain structure and another determines its overall sign. The magnetoelectric inversion of domain patterns is one of many imaginable examples of the as-yet-unexplored functionalities in systems with many complex order parameters.

Co_3TeO_6 forms monoclinic crystals (space group $C2/c1'$). Below 17.7 K, the magnetic order[9–11] is defined by two propagation vectors, $\boldsymbol{k}_0 = (0, 0, 0)$ and $\boldsymbol{k}_{\neq 0} \approx (0, 0.5, 0.25)$, which lead to order parameters $\zeta(\boldsymbol{k}_0)$ and $\eta(\boldsymbol{k}_{\neq 0})$, respectively (Methods, Extended Data Fig. 1)[12,13]. The magnetic point group symmetry is $2'$, which permits a spontaneous magnetization $M_{x,z}(\zeta(\boldsymbol{k}_0), \eta(\boldsymbol{k}_{\neq 0}))$ and a spontaneous polarization $P_y(\zeta(\boldsymbol{k}_0), \eta(\boldsymbol{k}_{\neq 0}))$. Experiments[9,10,12] yield $M_{x,z} = 0.57 \times 10^{-3} \mu_B$ per Co^{2+}, where μ_B is the Bohr magneton, but $P_y = 0$.

Mn_2GeO_4 forms orthorhombic crystals (space group $Pnma1'$). The multiferroic phase below 5.5 K is characterized by four magnetic order parameters associated with the coexisting magnetic propagation vectors $\boldsymbol{k}_0 = (0, 0, 0)$ and $\boldsymbol{k}_{\neq 0} = (\pm 0.136, \pm 0.211, 0)$. Two order parameters, $X_1(\boldsymbol{k}_0)$ and $X_3(\boldsymbol{k}_0)$, describe commensurate antiferromagnetic and ferromagnetic contributions, respectively, while two others, $M^{D1}(\boldsymbol{k}_{\neq 0})$ and $M^{D2}(\boldsymbol{k}_{\neq 0})$, describe incommensurate spiral components[6,14,15]. The magnetic point group symmetry is 2, and a spontaneous magnetization $M_z \propto X_3(\boldsymbol{k}_0)$ and a magnetically induced electric polarization $P_z \propto M^{D1,2}(\boldsymbol{k}_{\neq 0})$ coexist (Methods, Extended Data Fig. 2). Experiments[6,16] yield $M_z = 7 \times 10^{-3} \mu_B$ per Mn^{2+} and $P_z = 6\,\mu C\,m^{-2}$.

We image the spatial distributions of domains by using SHG—that is, frequency doubling of light in a material[7]. The relationship between the polarizations of the incident and emitted light, at frequencies ω and 2ω, respectively, depends on the symmetry of the material. Because any type of ferroic order changes the point group symmetry, characteristic SHG contributions emerge that allow us to image the associated domain patterns[8] with a resolution of about 1 μm. In particular, SHG detects the small spontaneous magnetization or polarization that is often associated with multiferroic materials (see Methods for details on the SHG coupling and experiment)[4].

SHG spectra from a z-oriented Co_3TeO_6 sample (Fig. 1a) yield maxima at 2.56 eV and 2.65 eV from electronic transitions within the Co^{2+} ($3d$) band. The polarization of the SHG light and its presence below 17.4 K (Fig. 1b) are in line with coupling to $M_{x,z}$ (Methods). We use this SHG signal to image the ferromagnetic $M_{x,z}$ domain distribution in a zero-field-cooled z-oriented Co_3TeO_6 sample. Interference with a crystallographic SHG background signal reveals domains at $+M_{x,z}$ and $-M_{x,z}$ as regions of different brightness in Fig. 1c (Methods).

In Fig. 2 we show the evolution of an $M_{x,z}$ domain structure for a magnetic field H_y, sweeping $\mu_0 H_y$ across the range −2.4 T to +2.4 T. Because $H_y \perp M_{x,z}$, the field does not convert the $\pm M_{x,z}$ domains into a single-domain state. Zero-field cooling reveals many domains, whereas the application of +2.4 T yields a simplified pattern with only a few dominant domains (Fig. 2b). When the field is reversed, the number of domains increases at around 0 T (Fig. 2c). However, at −2.4 T we obtain a domain pattern that is nearly identical to that at +2.4 T (Fig. 2b), but with the brightness of each domain inverted (Fig. 2d). Apparently, $M_{x,z}$ is reversed in each individual domain, but without affecting the shape

[1]Department of Materials, ETH Zurich, Zurich, Switzerland. [2]Laboratory for Multiscale Materials Experiments, Paul Scherrer Institut, Villigen, Switzerland. [3]Helmholtz-Institut für Strahlen- und Kernphysik, Universität Bonn, Bonn, Germany. [4]Laboratory for Neutron Scattering and Imaging, Paul Scherrer Institut, Villigen, Switzerland. [5]Department of Physics, Stockholm University, Stockholm, Sweden. [6]Physique des Systèmes Complexes, Université de Picardie, Amiens, France. [7]Institute of Materials Structure Science, High Energy Accelerator Research Organization (KEK), Tsukuba, Japan. [8]Department of Advanced Materials Science, University of Tokyo, Kashiwa, Japan. [9]Department of Multifunctional Materials, Karpov Institute of Physical Chemistry, Moscow, Russia. [10]Institute for Chemical Technology and Analytics, Division of Structural Chemistry, TU Wien, Vienna, Austria. [11]Department of Materials Science and Engineering, Norwegian University of Science and Technology (NTNU), Trondheim, Norway. [12]These authors contributed equally: N. Leo, V. Carolus. *e-mail: manfred.fiebig@mat.ethz.ch

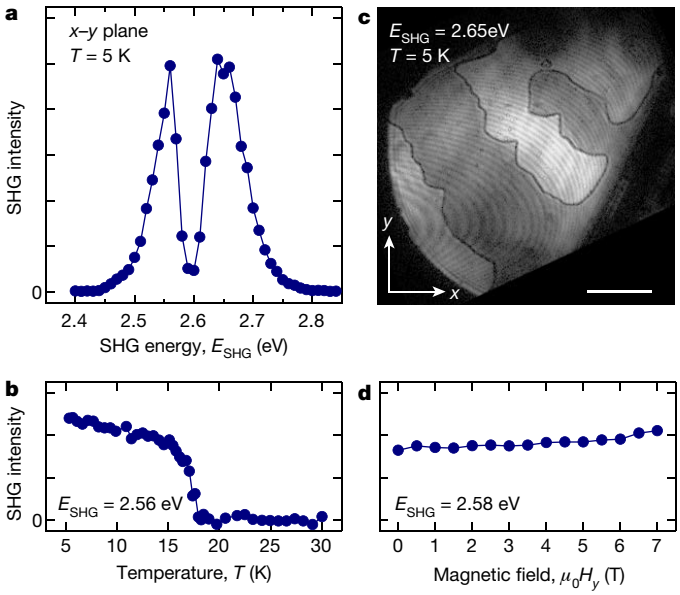

Fig. 1 | Probing ferromagnetism in Co_3TeO_6 by using SHG. a, SHG intensity spectrum at $T = 5$ K for x-polarized frequency-doubled and y-polarized incident light (proportional to the nonlinear susceptibility component χ_{xyy}) on a z-oriented sample. Henceforth, photon energies at the intensity maxima at $E_{SHG} = 2.56$ eV and $E_{SHG} = 2.65$ eV are used. Data noise in all SHG measurements is shot noise of the digital camera. All measurements were reproduced multiple times. **b**, Temperature dependence of the χ_{xyy}-related SHG intensity. The signal is observed in the magnetoelectric phase only below 17.4 K. **c**, Distribution of ferromagnetic domains in a z-oriented Co_3TeO_6 sample. An SHG interference technique visualizes the $\pm M_{x,z}$ domains as regions with different brightness (Methods, Extended Data Fig. 3). Scale bar, 500 μm. **d**, Dependence of the χ_{xyy}-related SHG intensity on a magnetic field H_y. μ_0 is the vacuum permeability. In contrast to the image in **c**, the SHG yield is independent of the domain state because the SHG interference technique that generates the contrast between opposite domain states in **c** is not applied. Thus, unperturbed by the domain state, **d** reveals the H_y dependence of the magnitude of $M_{x,z}$.

and distribution of the domains. We thus find a striking inversion of an entire inhomogeneous distribution of ferromagnetic domains by a homogeneous field.

The reversal occurs via intermittent formation and shifts of domain walls (Fig. 2c). This and the approximate H_y independence of the magnitude of $M_{x,z}$ (Fig. 1d) rule out the possibility that the brightness inversion is an optical artefact. Furthermore, the domain-wall mobility excludes the possibility that the protection of the domain pattern is caused by pinning effects. According to the magnetic-field dependence of the SHG interference shown in Fig. 2e, integrated over the range −3 T to +3 T over two spots of about 500 μm, the most substantial domain variations occur between −0.2 T and +0.2 T. The protection of the domain pattern at high fields is in stark contrast to its variability at low fields.

The inversion of the $M_{x,z}$ domain pattern by the homogeneous H_y field is resolved by a free-energy term that couples $M_{x,z}(\zeta(\boldsymbol{k}_0), \eta(\boldsymbol{k}_{\neq 0}))$ to H_y in a sign-sensitive way. An analysis of Landau invariants reveals the lowest-order term that enables such coupling as

$$F_{inv} \propto \mathcal{C}(\boldsymbol{k}_{\neq 0}) M_y(H_y) M_{x,z} \quad (1)$$

Here, $\mathcal{C}(\boldsymbol{k}_{\neq 0})$ is a product of the components of $\eta(\boldsymbol{k}_{\neq 0})$ that establishes the invariance of the free-energy contribution F_{inv} (see Methods for its derivation)[17]. Because a magnetic field H_y induces a proportional magnetization M_y and does not act on $\mathcal{C}(\boldsymbol{k}_{\neq 0})$, a reversal of $H_y \propto M_y$ entails reorientation of $M_{x,z}$ to retain $F_{inv} < 0$ for ground-state energy minimization. This sensitivity of the orientation of $M_{x,z}$ to H_y does not contradict the aforementioned near-insensitivity of the magnitude of $M_{x,z}$ to H_y, because these two properties originate from different coupling terms. Hence, the same order parameters that are responsible for magnetoelectric coupling in Co_3TeO_6 provide the basis for other intriguing cross-correlations, here the inversion of an entire ferromagnetic domain pattern.

To support our claim of generality for the domain-inversion behaviour, we now turn to Mn_2GeO_4, a material that differs from Co_3TeO_6 in crystal structure as well as magnetic and electric order. The SHG spectrum of a z-oriented Mn_2GeO_4 platelet (Fig. 3a) yields a peak at 1.83 eV. The signal is present in the multiferroic phase below 5.5 K (Fig. 3b), implying coupling to M_z or P_z. Zero-field cooling resolves many domains and domain walls (Fig. 3c), but application of an electric field $E_z = 144$ kV cm^{-1} transforms this phase into a single-domain state (Fig. 3d). By contrast, a magnetic field H_z above the coercive field leaves the sample in a multi-domain state (Fig. 4a). Therefore, we conclude that SHG couples to the spontaneous polarization P_z but not to the magnetization M_z.

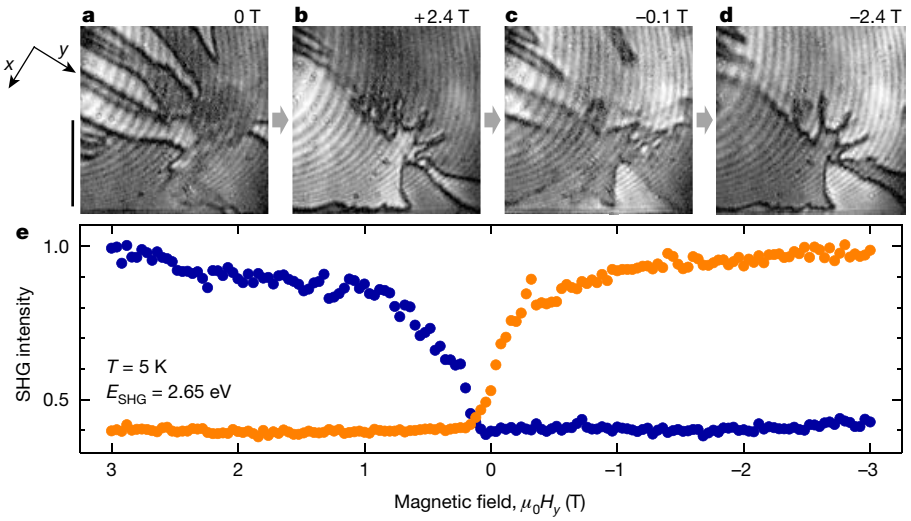

Fig. 2 | Inversion of the ferromagnetic domain pattern in Co_3TeO_6. **a**–**d**, Sequentially taken SHG images of the $\pm M_{x,z}$ domain pattern on a z-oriented Co_3TeO_6 sample at the given magnetic fields H_y. Scale bar, 500 μm. **e**, Dependence of the $M_{x,z}$ domain state on a magnetic field H_y. The domain-state-sensitive SHG interference (Methods) was measured on two spots of 500 μm diameter that lie in opposite domain states (blue and orange data points) outside the area shown in **a**–**d**. Tuning the magnetic field between positive and negative values reverses the magnetization of each domain while the domain pattern remains intact. The interchange is mainly limited to the field interval −0.2 T to +0.2 T. The inversion progresses via transient formation and shifts of domains and domain walls.

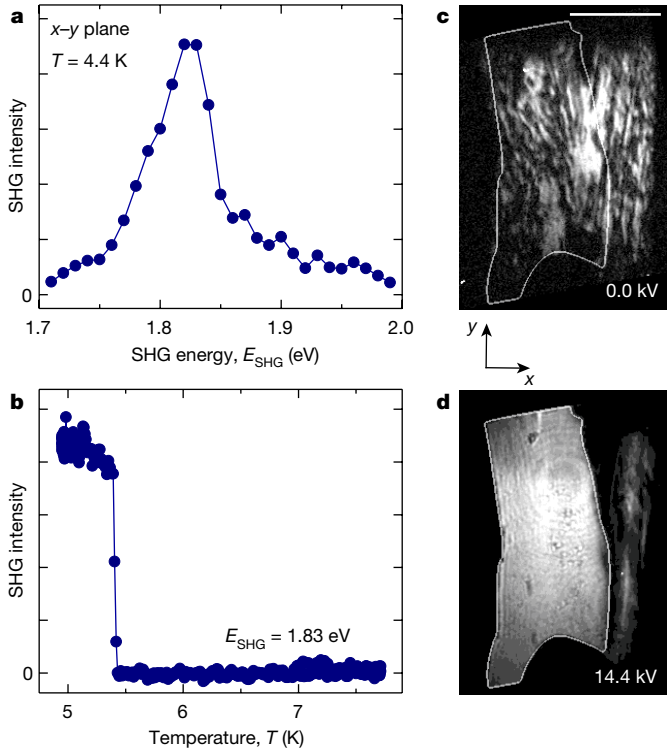

Fig. 3 | Probing ferroelectricity in Mn_2GeO_4 by using SHG. **a**, SHG intensity spectrum at $T = 4.4$ K for z-polarized frequency-doubled and y-polarized incident light (proportional to the nonlinear susceptibility component χ_{zyy}) on a z-oriented and slightly tilted sample. The peak at $E_{SHG} = 1.83$ eV identifies the photon energy that we used for the subsequent measurements. **b**, Temperature dependence of the χ_{zyy}-related SHG intensity after subtracting temperature-independent background contributions from the surface and higher-order-multipole SHG. A signal is observed in the multiferroic phase below 5.5 K. **c**, The domain structure of a zero-field-cooled sample reveals an inhomogeneous distribution of bright and dark regions, indicating a large number of domains and domain walls. Scale bar, 500 μm. **d**, After applying an electric field $E_z = 144$ kV cm^{-1}, the SHG image exhibits homogeneous brightness, indicating a ferroelectric single-domain state in the region in which the transparent electrodes overlap (white outline).

The evolution of the ferroelectric P_z domains with an applied magnetic field H_z is shown in Fig. 4. First, the sample is field-cooled at $H_z = -230$ mT, which induces a single-domain $-M_z$ state[6], but, according to the SHG image at $H_z = 0$ in Fig. 4a, retains a ferroelectric multi-domain state. As H_z is increased towards positive values, additional ferroelectric domain walls are formed and move across the sample. At +150 mT we obtain a ferroelectric domain pattern that is nearly identical to the one observed initially, except that P_z in each domain is reversed (Fig. 4h). Increasing H_z yields no additional change, and further field cycles corroborate the reproducibility of the local P_z inversion without changes to the domain pattern.

We thus encounter a situation for the ferroelectric order in Mn_2GeO_4 that is analogous to the ferromagnetic order of Co_3TeO_6. The order in each domain is reversed, but the domain pattern is unchanged—a phenomenon that goes beyond the magnetoelectric switching between single-domain states discussed so far[6,18]. To explain the domain inversion in Mn_2GeO_4, we require a sign-sensitive coupling between P_z and H_z. An analysis of Landau invariants involving the order parameters $X_{1,3}(\boldsymbol{k}_0)$ and $M^{D1,2}(\boldsymbol{k}_{\neq 0})$ reveals

$$F_{inv} \propto \mathcal{C}(\boldsymbol{k}_0) M_z(H_z) P_z \quad (2)$$

with $\mathcal{C}(\boldsymbol{k}_0) \propto X_1(\boldsymbol{k}_0)$ (see Methods for the Landau theory developed by Harris)[14,15]. Cooling in a magnetic field H_z sets a uniform magnetization $M_z \propto H_z$. This still allows a $\pm P_z$ domain distribution because $F_{inv} < 0$ can be retained by the sign of $\mathcal{C}(\boldsymbol{k}_0)$. Because $\mathcal{C}(\boldsymbol{k}_0)$ remains invariant under the application of H_z, the free energy is minimized only if P_z switches simultaneously with the reversal of $M_z \propto H_z$. Thus, in two different materials, we have demonstrated the inversion of ferromagnetic or ferroelectric domain patterns with a single sweep of a homogeneous, non-conjugated field.

To generalize our two examples, Co_3TeO_6 and Mn_2GeO_4, we express the inversion using a trilinear coupling term in the free energy:

$$F_{inv} \propto \hat{I}\hat{S}(H_S)\hat{O} \quad (3)$$

The effect of this coupling term is illustrated in Fig. 5. $\hat{O}$ represents the experimentally observed domain distribution (magnetization or polarization). $\hat{I}$ contains the memory of the domain pattern that is preserved, because it remains invariant under the applied field H_S. By contrast, $\hat{S} = \hat{S}(H_S)$ can be switched by H_S. For $H_S \ll 0$, $\hat{S}$ is in a single-domain -1 state and the observable $\hat{O}$ assumes the domain structure of $\hat{I}$. When

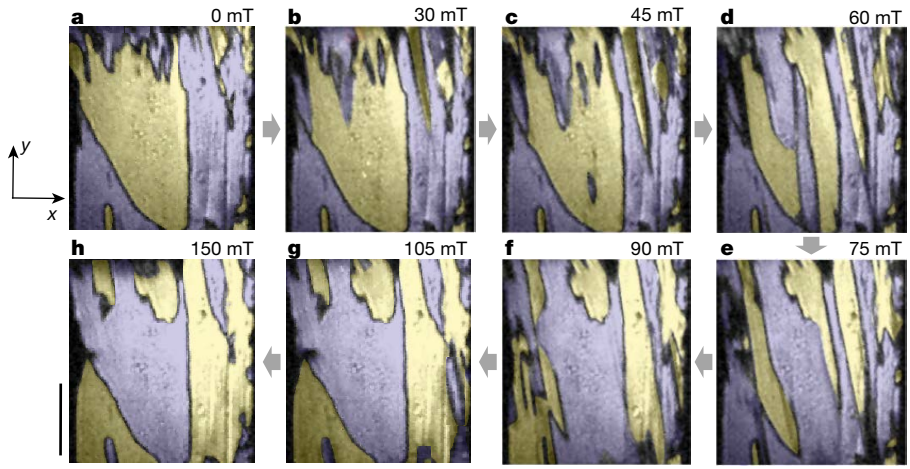

Fig. 4 | Inversion of the ferroelectric domain pattern in Mn_2GeO_4. Sequentially taken SHG images of $\pm P_z$ domains on a z-oriented Mn_2GeO_4 sample at the given magnetic fields H_z (see Extended Data Fig. 4 for the corresponding experiment on an x-oriented sample). Because of the small SHG contrast, domain states at $+P_z$ and $-P_z$ are highlighted by yellow and purple shading, respectively. Scale bar, 500 μm. **a**, After field-cooling at $\mu_0 H_z = -230$ mT, followed by setting $\mu_0 H_z = 0$, the sample is in a ferroelectric multi-domain state. **b**–**g**, Application of $\mu_0 H_z > 0$ leads to additional nucleation and movement of domain walls. **h**, In the saturated state at +150 mT, almost the same domain distribution as in **a** (after the original field cooling) is obtained, but with the orientation of the ferroelectric polarization reversed in each domain.

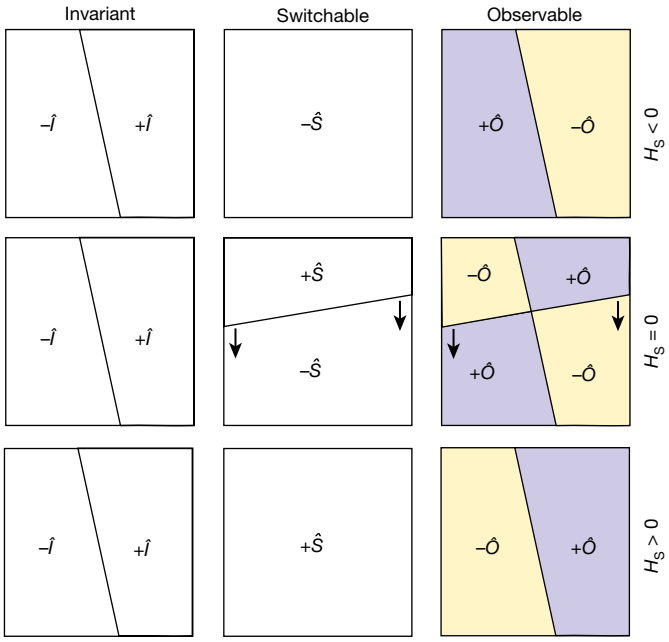

Fig. 5 | Multi-order-parameter model for domain-pattern inversion. $\hat{O}$ represents the domain distribution observed in the experiment: magnetization for Co_3TeO_6 or polarization for Mn_2GeO_4 (reflected in Fig. 4 by the colour shading). $\hat{I}$ contains the memory of the domain pattern to be preserved in $\hat{O}$. Then, $\hat{S} = \hat{S}(H_S)$ is switched between a uniform -1 state and a uniform $+1$ state by ramping the applied field H_S between its maximum negative and positive values. Reversal of $\hat{S}$ by H_S entails reversal of $\hat{O}$ to minimize the free energy in equation (3), because $\hat{I}$ is immutable under H_S. Thus, the field H_S reverses the orientation of the order parameter of $\hat{O}$ in each domain, but preserves the domain structure. When crossing $H_S = 0$, $\hat{S}$ enters a transient multi-domain state with the nucleation and propagation of $(-1)/(+1)$ domain walls. This leads to the observed transient increase in the number of domain walls and their propagation in $\hat{O}$. The propagation of $\hat{O}$ and $\hat{S}$ domain walls is indicated by arrows. The sample-specific expressions for $\hat{I}$, $\hat{S}$ and $\hat{O}$ are listed in Table 1.

crossing $H_S = 0$, $\hat{S}$ becomes transiently multi-domain; consequently, new domain walls appear in $\hat{O}$ and propagate across the sample. For $H_S \gg 0$, $\hat{S}$ resumes the single-domain state (now $+1$) and the initial domain configuration of $\hat{I}$ is recovered in $\hat{O}$, albeit with the orientation of $\hat{O}$ reversed in each domain because of the H_S-controlled sign change of $\hat{S}$. The deterministic interchange of domain patterns expressed by equation (3) distinguishes our experiment from the non-deterministic switching between multi-domain patterns found, for example, in partial ferroics[19]. The expressions for $\hat{I}$, $\hat{S}$ and $\hat{O}$ are sample-specific (Table 1, Methods); however, supported by the independence of our two chosen examples, Co_3TeO_6 and Mn_2GeO_4, we argue that the inherent complexity of any system that is characterized by several multidimensional order parameters at different magnetic propagation vectors $\boldsymbol{k}$ makes their widespread existence and coupling likely.

Multiferroics are ideal for domain-pattern inversion because of the inherent order-parameter complexity required to achieve strongly coupled magnetic and electric order. $CoCr_2O_4$ or, at room temperature, hexaferrites may be candidates for such inversion[18,20–22]. Aside from symmetry, material parameters need to be satisfied. Coupling between $\hat{I}$ and $\hat{S}$ beyond that in equation (3), such as by strain, must be small. Furthermore, the $\hat{I}$ walls must not pin the motion of the $\hat{S}$ walls during the inversion. On the other hand, an alternative domain-inversion mechanism to the one presented here may be entirely rooted in domain-wall coupling and be absent within the domains. $GdFeO_3$ or the hexagonal manganites are possible candidates for this behaviour[18,23]. These other examples confirm the idea that we have presented only one of many conceivable examples of order-parameter coupling beyond magnetoelectric phase control; many other multi-order-parameter functionalities remain to be explored.

Table 1 | Material-specific terms and order parameters

Material	$\hat{I}$	$\hat{S}(H_S)$	$\hat{O}$
Co_3TeO_6	$\mathcal{C}(\boldsymbol{k}_{\neq 0}) \mapsto \eta$	$M_y(H_y) \mapsto \zeta$	$M_{x,z} \mapsto \eta, \zeta$
Mn_2GeO_4	$\mathcal{C}(\boldsymbol{k}_0) \mapsto X_1$	$M_z(H_z) \mapsto X_3$	$P_z \mapsto X_1, X_3$

The table shows the values of the terms $\hat{I}$, $\hat{S}(H_S)$ and $\hat{O}$ in equations (1) and (2) and their relationship to the order parameters of Co_3TeO_6 and Mn_2GeO_4, respectively. See Methods for explicit definitions of the order parameters and of $\hat{I}$, $\hat{S}$ and $\hat{O}$.

Online content

Any methods, additional references, Nature Research reporting summaries, source data, statements of data availability and associated accession codes are available at https://doi.org/10.1038/s41586-018-0432-4

Received: 13 February; Accepted: 27 June 2018;
Published online 22 August 2018.

1. Hansen, C. H. *Understanding Active Noise Cancelation* (Spon Press, New York, 2001).
2. Jung, B. A. & Weigel, M. Spin echo magnetic resonance imaging. *J. Magn. Reson. Imaging* **37**, 805–817 (2013).
3. Wang, K. F., Liuab, J.-M. & Renc, Z. F. Multiferroicity: the coupling between magnetic and polarization orders. *Adv. Phys.* **58**, 321–448 (2009).
4. Fiebig, M., Lottermoser, Th., Meier, M. & Trassin, M. The evolution of multiferroics. *Nat. Rev. Mater.* **1**, 16046 (2016).
5. Benedek, N. A. & Fennie, C. J. Hybrid improper ferroelectricity: a mechanism for controllable polarization-magnetization coupling. *Phys. Rev. Lett.* **106**, 107204 (2011).
6. White, J. S. et al. Coupling of magnetic and ferroelectric hysteresis by a multicomponent magnetic structure in Mn_2GeO_4. *Phys. Rev. Lett.* **108**, 077204 (2012).
7. Pershan, P. S. Nonlinear optical properties of solids: energy considerations. *Phys. Rev.* **130**, 919–929 (1963).
8. Fiebig, M., Pavlov, V. V. & Pisarev, R. V. Second-harmonic generation as a tool for studying electronic and magnetic structures of crystals. *J. Opt. Soc. Am. B* **22**, 96–118 (2005).
9. Singh, H. et al. Short range ferromagnetic, magneto-electric, and magneto-dielectric effect in ceramic Co_3TeO_6. *J. Appl. Phys.* **119**, 044104 (2016).
10. Hudl, M. et al. Complex magnetism and magnetic-field-driven electrical polarization in Co_3TeO_6. *Phys. Rev. B* **84**, 180404 (2011).
11. Li, W.-H. et al. Interplay between the magnetic and electric degrees of freedom in multiferroic Co_3TeO_6. *Phys. Rev. B* **85**, 094431 (2012).
12. Tolédano, P. et al. First-order multi-k phase transitions and magnetoelectric effects in multiferroic Co_3TeO_6. *Phys. Rev. B* **85**, 214439 (2012).
13. Ivanov, S. A. et al. Temperature-dependent multi-k magnetic structure in multiferroic Co_3TeO_6. *Mater. Res. Bull.* **47**, 63–72 (2012).
14. Honda, T. et al. Coupled multiferroic domain switching in the canted conical spin spiral system Mn_2GeO_4. *Nat. Commun.* **8**, 15457 (2017).
15. Harris, A. B. Identifying Landau order parameters and their transformation properties for complex multiferroics: the case of Mn_2GeO_4. *Phys. Rev. B* **96**, 054422 (2017).
16. Honda, T., Ishiguro, Y., Nakamura, H., Wakabayashi, Y. & Kimura, T. Structure and magnetic phase diagrams of multiferroic Mn_2GeO_4. *J. Phys. Soc. Jpn.* **81**, 103703 (2012).
17. Carolus, V. *Topography and Manipulation of Magnetic Domains in Cobalt Tellurite*. PhD thesis, Bonn Univ. (2014).
18. Tokunaga, Y. et al. Composite domain walls in a multiferroic perovskite ferrite. *Nat. Mater.* **8**, 558–562 (2009).
19. Aizu, K. Possible species of ferromagnetic, ferroelectric, and ferroelastic crystals. *Phys. Rev. B* **2**, 754–772 (1970).
20. Yamasaki, Y. et al. Magnetic reversal of the ferroelectric polarization in a multiferroic spinel oxide. *Phys. Rev. Lett.* **96**, 207204 (2006).
21. Tokunaga, Y. et al. Multiferroic M-type hexaferrites with a room-temperature conical state and magnetically controllable spin helicity. *Phys. Rev. Lett.* **105**, 257201 (2010).
22. Zhai, K. et al. Giant magnetoelectric effects achieved by tuning spin cone symmetry in Y-type hexaferrites. *Nat. Commun.* **8**, 51 (2017).
23. Fiebig, M., Lottermoser, Th., Fröhlich, D., Goltsev, A. V. & Pisarev, R. V. Observation of coupled magnetic and electric domains. *Nature* **419**, 818–820 (2002).

Acknowledgements J.S.W. thanks the SNSF for support via grant 200021_153451. M.K. acknowledges financial support by SNSF grant 200021_165855. S.A.I. acknowledges financial support from the Russian Foundation for Basic Research. M.F. is grateful for support by SNSF grant 200021_178825. We thank B. Harris for a discussion of the Landau theory for Mn_2GeO_4 in refs [14,15], prior to their publication.

Reviewer information *Nature* thanks V. Gopalan and the other anonymous reviewer(s) for their contribution to the peer review of this work.

Author contributions All authors contributed to the discussion and interpretation of the experiment and to the completion of the manuscript. N.L. and V.C. performed the experiments. N.L., J.S.W. and M.K. interpreted the domain-pattern inversion on the basis of a previously published[14,15] Landau-theoretical description of the order parameters. V.C., M.H. and P.T. performed the Landau-theoretical analysis of the Co_3TeO_6 experiments. M.W. grew single crystals of Co_3TeO_6 and S.A.I. analysed their stoichiometry and structure. T.H. and T.K. prepared single crystals of Mn_2GeO_4. Th.L. supervised the experiments on Co_3TeO_6. D.M. and M.F. initiated the experiment and supervised the work.

Competing interests The authors declare no competing interests.

Additional information
Extended data is available for this paper at https://doi.org/10.1038/s41586-018-0432-4.
Reprints and permissions information is available at http://www.nature.com/reprints.
Correspondence and requests for materials should be addressed to M.F.
Publisher's note: Springer Nature remains neutral with regard to jurisdictional claims in published maps and institutional affiliations.

METHODS

Sample preparation. Single crystals of Co_3TeO_6 were grown by using the chemical vapour transport method. The chemical composition and the homogeneity of the crystals were analysed by using energy-dispersive spectroscopy using a JEOL 840A scanning electron microscope and INCA 4.07 (Oxford Instruments) software. For the sample prepared for diffraction measurements, the cation content was also determined by inductively coupled plasma atomic emission spectroscopy performed with an ARL Fisions 3410 spectrometer. According to the elemental analysis done on 20 different crystallites, the stoichiometry is $Co_{2.98(3)}$, $Te_{1.02(3)}$ and $O_{5.99(2)}$ (oxygen value derived from iodometric titration). A room-temperature X-ray diffraction pattern on a Bruker D8 Advance diffractometer yielded $a = 14.8117(4)$ Å, $b = 8.8392(3)$ Å, $c = 10.3587(4)$ Å and $\beta = 94.84(1)°$ as monoclinic unit-cell parameters. Single crystals of Mn_2GeO_4 were grown by using the floating-zone method as described elsewhere[13,16]. All crystals were oriented by using Laue diffraction, cut, lapped to a thickness of about 50 μm and polished from both sides with silica slurry.

Second-harmonic generation (SHG). SHG denotes the doubling of the frequency of a light wave in a material. Restricting ourselves to the (leading) electric-dipole approximation, SHG is described by[7] $P_i(2\omega) \propto \chi_{ijk}E_j(\omega)E_k(\omega)$. Here, $E_{j,k}(\omega)$ denote the electric-field components of the incident light and $P_i(2\omega)$ is the induced i-polarized nonlinear polarization that acts as source for the emitted SHG wave at intensity $I \propto |\boldsymbol{P}(2\omega)|^2$. The nonlinear susceptibility tensor χ characterizes the symmetry of the host material[24]. Because ferroic order changes the point group symmetry, it leads to the emergence of ordering-induced contributions to the SHG yield, which we use to probe this order with spectral and spatial resolution[8]. Domain states with opposite orientation of the order parameter differ in the sign of the corresponding SHG light waves, equivalent to a 180° phase shift. This allows us to image opposite domain states as regions of different brightness via an interference technique[25] illustrated in Extended Data Fig. 3. The detailed set-up for transmission SHG experiments is described elsewhere[8].

SHG experiments on Co_3TeO_6. The 2′ magnetic point group symmetry of the phase below 17.4 K permits a set of time-reversal-symmetry-violating ('c-type') electric-dipole SHG contributions proportional to $M_{x,z}$. According to symmetry tables[24], this set includes 14 tensor components. We observed all of these and verified that they display the same $M_{x,z}$-related temperature dependence as in Fig. 1b. In turn, no other tensor components yielding an order parameter coupling were identified, consistent with the 2′ point group symmetry and the earlier observation that P_y, although allowed, is measured as zero[9,10,12]. According to theory, the coupling to the magnetic order parameter by SHG is typically the result of the low-symmetry environment of the paramagnetic ions in combination with spin–orbit interaction[8]. Experiments were performed in a liquid-helium-operated split-coil magnetic-field cryostat on a z-cut sample with light in perpendicular incidence. We used light pulses of 5 ns emitted from an optical parametric oscillator pumped by the frequency-tripled light emitted from a Nd:YAG laser. Superposition of the SHG wave from the χ_{xyy} component with a constant crystallographic SHG reference contribution from the χ_{yyy} component was used for the aforementioned interference technique that identifies opposite domain states by their different brightness[25].

SHG experiments on Mn_2GeO_4. The 2 point group symmetry of the multiferroic phase below 5.5 K allows a set of time-reversal-symmetry-conserving ('i-type') electric-dipole SHG contributions proportional to P_z. This set includes 13 components[24], from which we selected χ_{zyy} and χ_{yyz}. Experiments were performed on a z-cut sample onto which transparent electrodes were sputtered to apply large electric fields. To access the z-polarized SHG contribution in χ_{zyy}, the sample was tilted with respect to the direction of the incident light. In addition, we show experiments for χ_{yyz} on an x-cut sample in Extended Data Fig. 4. We used light pulses of 120 fs emitted from an optical parametric amplifier pumped by an amplified Ti:sapphire laser system. Destructive interference of SHG waves from opposite $\pm P_z$ domain states at the position of the domain walls reveals the domain boundaries as black lines meandering through the SHG image[26]. These are used to identify the ferroelectric domain pattern.

Landau theory for the low-temperature phase of Co_3TeO_6. Here we provide the link between our qualitative treatment of the propagation vectors, order parameters and invariants that describe the magnetoelectric order of Co_3TeO_6 and the full group-theoretical derivation; see also refs [12,17] for the latter. Using the notation of ref. [12], the phase of Co_3TeO_6 below 17.4 K is characterized by two magnetic order parameters associated with the coexisting magnetic modulations vectors $\boldsymbol{k}_0 = \boldsymbol{k}_2 = (0, 0, 0)$ and $\boldsymbol{k}_{\neq 0} = \boldsymbol{k}_3 \approx (0, 0.5, 0.25)$ (ref. [13]). $\boldsymbol{k}_0$ is associated with the one-dimensional magnetic order parameter $\zeta(\boldsymbol{k}_0)$ and from the one-dimensional little group of the four-armed star of $\boldsymbol{k}_{\neq 0}$ we can construct the four-dimensional order parameter $\eta(\boldsymbol{k}_{\neq 0}) = (\rho_1 e^{i\theta_1}, \rho_1 e^{-i\theta_1}, \rho_2 e^{i\theta_2}, \rho_2 e^{-i\theta_2})$ (ref. [12]). The latter is simplified by assuming $\rho_1 = \rho_2 = \rho_e$ and $\theta_1 = \theta_2 = \theta_e$ because of the (approximate[11]) commensurability of $\boldsymbol{k}_{\neq 0}$. The coexisting antiferromagnetic order parameters $\zeta(\boldsymbol{k}_0)$ and $\eta(\boldsymbol{k}_{\neq 0})$ yield the magnetic point group symmetry 2′, which permits a spontaneous magnetization $M_{x,z} \propto \zeta\rho_e^4\cos(4\theta_e)$ and a spontaneous electric polarization $P_y \propto \zeta^2\rho_e^4\cos(4\theta_e)$. However, the latter was not detected at zero magnetic field, which indicates that Co_3TeO_6 is a magnetoelectric rather than a multiferroic compound[10,12].

To explain the inversion of the $M_{x,z}$ domains under the application of a magnetic field H_y, we require a coupling connecting $M_{x,y}(\zeta(\boldsymbol{k}_0),\eta(\boldsymbol{k}_{\neq 0}))$ and $M_y(H_y)$ in a sign-sensitive way that complies with the invariance of the free energy under the symmetry operations of the parent phase. In particular, translational invariance poses the following restrictive constraint: for order parameters at incommensurate propagation vectors, here $\boldsymbol{k}_{\neq 0}$, translational invariance can be retained only if these order parameters enter the free energy in even powers. However, the even power preserves time-reversal symmetry so that another—time-reversal-symmetry-violating—order parameter associated with a commensurate propagation vector, here $\boldsymbol{k}_0$, has to enter the trilinear term in equation (1).

Using the transformation behaviour of the order parameters $\eta(\boldsymbol{k}_{\neq 0})$ and $\zeta(\boldsymbol{k}_0)$, described by the irreducible representations[12] $\tau_1(\boldsymbol{k}_{\neq 0})$ and $\Gamma_4(\boldsymbol{k}_{\neq 0})$, respectively, we find $F_{\text{inv}} \propto \sigma_4(\boldsymbol{k}_{\neq 0})\zeta(\boldsymbol{k}_0)M_y(H_y)$ as the simplest coupling term to the free energy. Here, $\sigma_4(\boldsymbol{k}_{\neq 0}) = [\rho_1^4\sin(4\theta_1) - \rho_2^4\sin(4\theta_2)]$ is a fourth-order product of the elements of $\eta(\boldsymbol{k}_{\neq 0})$, which transforms like the irreducible representation $\tau_1(\boldsymbol{k}_{\neq 0})$ and retains the invariance of F_{inv}. Because $M_{x,z} \propto \zeta(\boldsymbol{k}_0)$, we have thus reconstructed the expression in equation (1), finding $\mathcal{C}(\boldsymbol{k}_{\neq 0}) = \sigma_4/[\rho_e^4\cos(4\theta_e)]$. Note that $\sigma_4(\boldsymbol{k}_{\neq 0})$ is non-zero only if $\boldsymbol{k}_{\neq 0}$ is incommensurate so that the degeneracy of ρ_e and θ_e is lifted (that is, $\rho_1 \neq \rho_2$ and $\theta_1 \neq \theta_2$). A small incommensurate modulation was indeed observed[11] in Co_3TeO_6, but is usually neglected because of the smallness of this correction[12]. However, in the domain-inversion mechanism, this correction generates the leading-order coupling term.

Landau theory for the multiferroic phase of Mn_2GeO_4. Here we provide the link between the qualitative treatment of the propagation vectors, order parameters and invariants that describe the magnetoelectric order of Mn_2GeO_4 and the full group-theoretical derivation; see also refs [14,15] for the latter. Using the notation of refs [14,15], the multiferroic phase of Mn_2GeO_4 below 5.5 K is characterized by four magnetic order parameters associated with the coexisting magnetic modulation vectors $\boldsymbol{k}_0 = \boldsymbol{Q}_c = (0, 0, 0)$ and $\boldsymbol{k}_{\neq 0} = \boldsymbol{Q}_{ic} = (\pm 0.136, \pm 0.211, 0)$. The two one-dimensional order parameters related to $\boldsymbol{k}_{\neq 0}$ are X_1 and X_3. From the two-dimensional little group of the four-armed star of $\boldsymbol{k}_{\neq 0}$ we can construct two four-dimensional magnetic order parameters M_Q^{D1} and M_Q^{D2} with $M_Q^{Di} = (M_{QA}^{Di}, M_{QB}^{Di}, M_{QA}^{Di*}, M_{QB}^{Di*})$ and $i = 1, 2$. Here A and B refer to the two possible directions of the magnetic propagation vector $\boldsymbol{k}_{\neq 0}$. The corresponding magnetic point group[6,14–16] is 2. Antiferromagnetic components proportional to $X_1(\boldsymbol{k}_0)$ and a spontaneous magnetization $M_z \propto X_3(\boldsymbol{k}_0)$ coexist with a spontaneous electric polarization $P_z \propto A_{ic} - B_{ic}$ so that $P_z \parallel M_z$ (corresponding to the term U in refs [14,15]). Here, $J_{ic} = M_{QJ}^{D1}M_{QJ}^{D2*} - M_{QJ}^{D1*}M_{QJ}^{D2}$ for $J = $ A, B.

For the domain inversion, a sign-sensitive coupling of $P_z(\boldsymbol{k}_{\neq 0})$ to H_z, and thus $M_z(H_z)(\boldsymbol{k}_0)$, is required. The lowest-order contribution that permits this is $F_{\text{inv}} \propto X_1X_3(A_{ic}^2 - B_{ic}^2) \propto X_1(A_{ic} + B_{ic})M_zP_z$. This reconstructs the expression in equation (2), yielding $\mathcal{C}(\boldsymbol{k}_0) = X_1(A_{ic} + B_{ic})$, and corresponds to the term W in refs [14,15]. Note that $\mathcal{C}(\boldsymbol{k}_0)$ contains contributions associated with $\boldsymbol{k}_0$ and $\boldsymbol{k}_{\neq 0}$. However, the term $A_{ic} + B_{ic} \propto \boldsymbol{k}_{\neq 0}$ merely retains the correct symmetry of the coupling, whereas $X_1(\boldsymbol{k}_0)$ holds the domain structure that determines the parallel or antiparallel orientation of M_z and P_z such that $F_{\text{inv}} < 0$ (refs [14,15]). Reversal of the field H_z reverses the magnetization M_z. Microscopically, this swaps the orientation of the Mn^{2+} spin cones (Extended Data Fig. 2), corresponding to an exchange of A_{ic} and B_{ic}. Because $P_z \propto A_{ic} - B_{ic}$, this simultaneously reverses the direction of polarization[14,15].

Data availability. The data that support the findings of this study are available from the corresponding author on reasonable request.

24. Birss, R. R. *Symmetry and Magnetism* Ch. 2, 3 (North-Holland, Amsterdam, 1966).
25. Leute, S., Lottermoser, Th. & Fröhlich, D. Nonlinear spatially resolved phase spectroscopy. *Opt. Lett.* **24**, 1520–1522 (1999).
26. Fiebig, M., Fröhlich, D., Lottermoser, Th. & Maat, M. Probing of ferroelectric surface and bulk domains in ferroelectric $R\text{MnO}_3$ (R = Y, Ho) by second harmonic generation. *Phys. Rev. B* **66**, 144102 (2002).

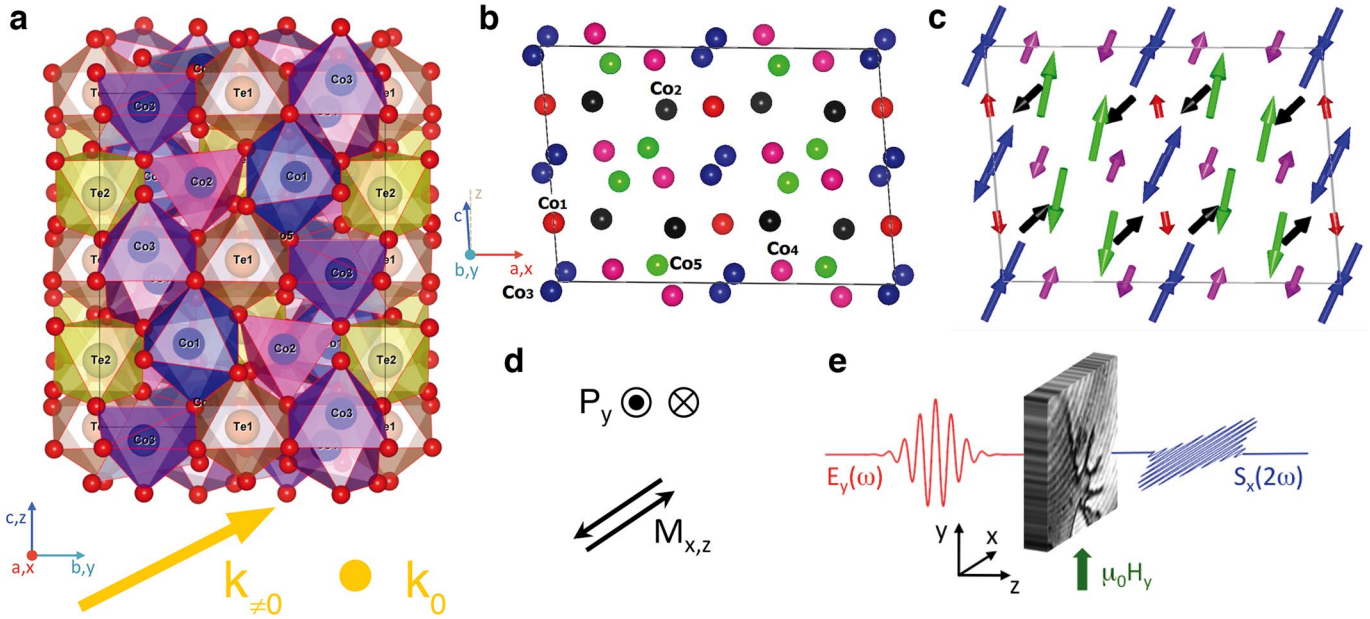

Extended Data Fig. 1 | Crystallographic structure, magnetic structure and optical excitation of Co_3TeO_6. a, Three-dimensional view of the crystallographic unit cell along the *x* axis in relation to the magnetic propagation vectors $\boldsymbol{k}_0$ and $\boldsymbol{k}_{\neq 0}$. **b**, Section of the unit cell in the *x*–*z* plane showing the location of the paramagnetic Co^{2+} ions in five different positions. **c**, Magnetic moments of the Co^{2+} ions shown in **b**. **d**, Orientation of the spontaneous magnetization $M_{x,z}$ and the electric polarization P_y. The latter is symmetry-allowed as spontaneous polarization, yet observed only as a magnetic-field-induced contribution[9,10,12]. **e**, Geometry of the SHG transmission experiment with light at ω and 2ω propagating along the *z* axis, probing a *z*-cut Co_3TeO_6 platelet in perpendicular incidence. The sample is exposed to a magnetic field H_y.

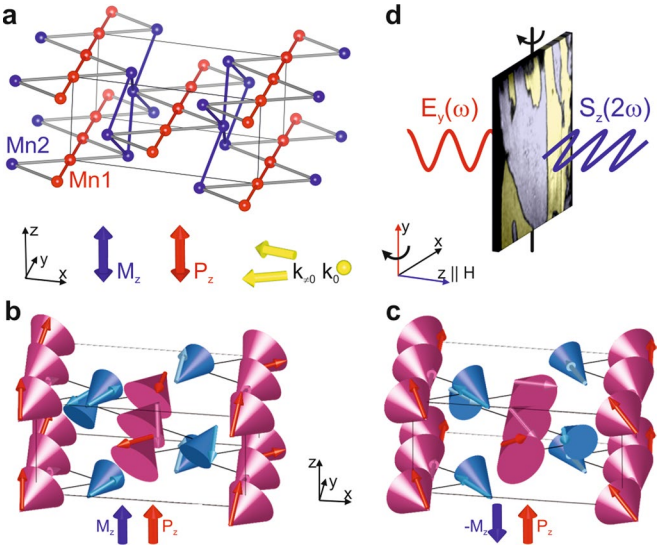

Extended Data Fig. 2 | Crystallographic structure, magnetic structure and optical excitation for Mn_2GeO_4. a, Top, three-dimensional view of the crystallographic unit cell showing the location of the paramagnetic Mn^{2+} ions on the different positions 'Mn1' and 'Mn2'. Bottom, orientation of the spontaneous magnetization M_z and spontaneous polarization P_z in relation to the magnetic propagation vectors $\boldsymbol{k}_0$ and $\boldsymbol{k}_{\neq 0}$. **b**, Conically modulated order of the magnetic Mn^{2+} moments on the Mn1 and Mn2 positions. Bold arrows show the resulting spontaneous magnetization M_z and spontaneous polarization P_z. **c**, As in **b**, but for reversed spontaneous magnetization. **d**, Geometry of the SHG transmission experiment with light incident onto a z-cut Mn_2GeO_4 platelet. The sample is exposed to a magnetic field H_z and it is rotated around the y axis so that the optical excitation does not occur in perpendicular geometry.

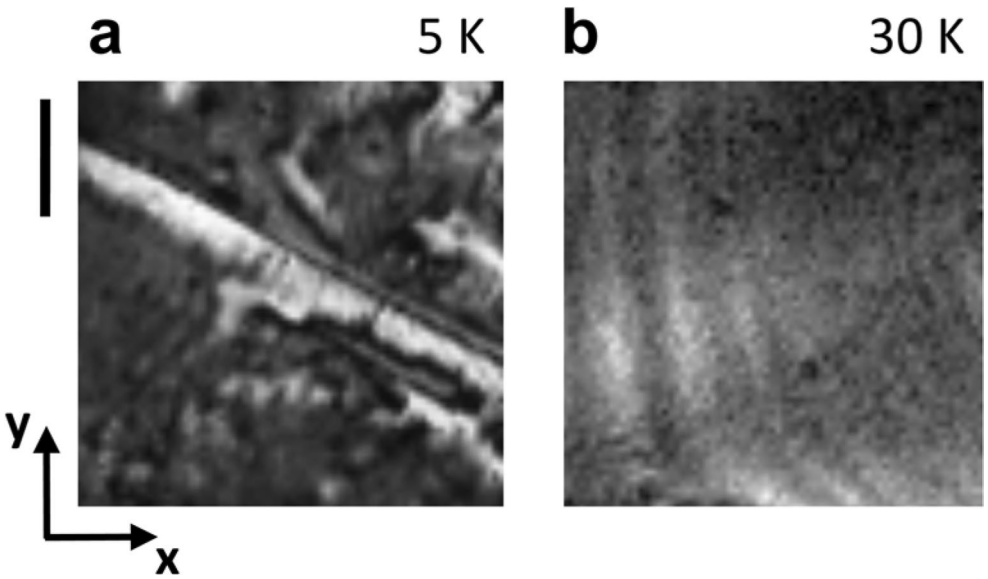

Extended Data Fig. 3 | SHG coupling and interference. a, Spatially resolved SHG image of a *z*-cut Co_3TeO_6 sample. At 5 K, a magnetization-induced SHG contribution from χ_{xyy} and a crystallographically induced SHG contribution from χ_{yyy} are present. The χ_{xyy} light waves from opposite domains differ by 180° because of proportionality to the spontaneous magnetization $\pm M_{x,z}$. The phase of the χ_{yyy} wave is homogeneous across the sample because it is blind to the magnetic order. Constructive ($+M_{x,z}$) and destructive ($-M_{x,z}$) interference of the magnetic and crystallographic SHG contributions therefore yields the opposite magnetic domain states as regions of different brightness. **b**, Image of the same region as in **a** but at 30 K, at which $M_{x,z} = 0$ so that only the homogeneous crystallographic SHG contribution from χ_{yyy} remains. Scale bar, 500 μm.

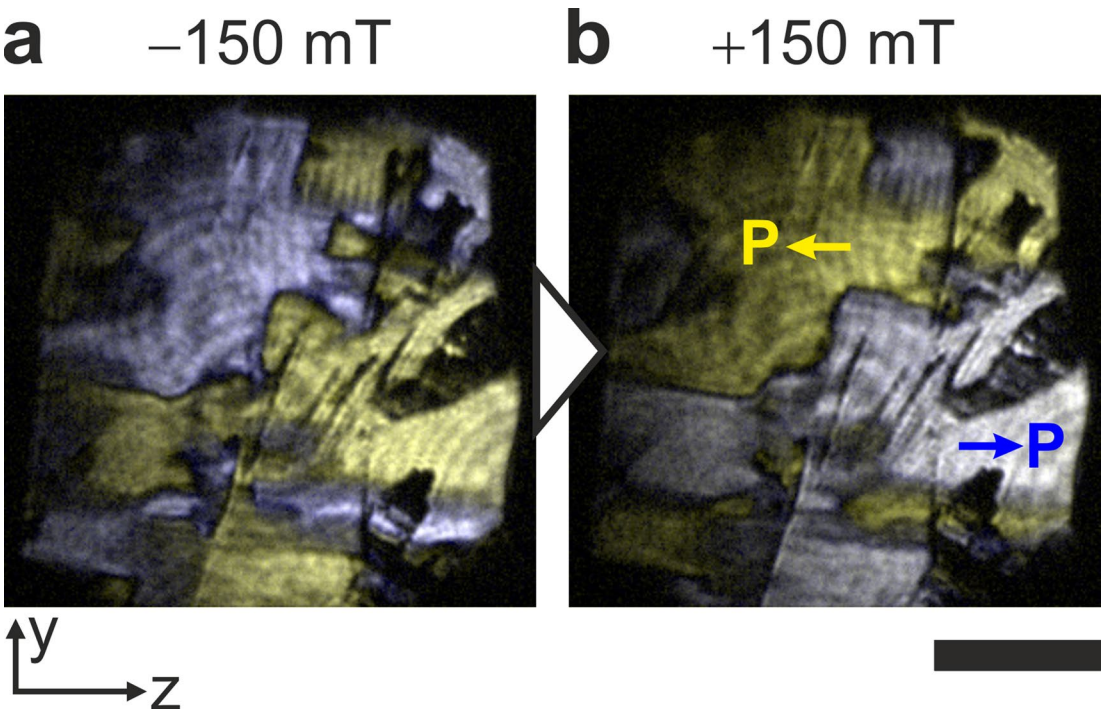

Extended Data Fig. 4 | Inversion of the ferroelectric domain pattern in an *x*-cut Mn_2GeO_4 sample. Sequentially taken SHG images of $\pm P_z$ domains on an *x*-oriented Mn_2GeO_4 sample at the given magnetic fields H_z. The same domain-inversion behaviour as for the *z*-cut sample in Fig. 4 is observed. Because of the small SHG contrast, opposite polarization domain states are highlighted by colour shading. Darker or black areas are caused by cracks and pores in the Mn_2GeO_4 sample. Scale bar, 500 μm.